International Journal of Radiation Oncology biology • physics

www.redjournal.org

Physics Contribution

Exploratory Investigation of Dose-Linear Energy Transfer (LET) Volume Histogram (DLVH) for Adverse Events Study in Intensity Modulated Proton Therapy (IMPT)

Yunze Yang, PhD,* Carlos E. Vargas, MD,* Ronik S. Bhangoo, MD,* William W. Wong, MD,* Steven E. Schild, MD,* Thomas B. Daniels, MD,* Sameer R. Keole, MD,* Jean-Claude M. Rwigema, MD,* Jennifer L. Glass, MS,* Jiajian Shen, PhD,* Todd A. DeWees, PhD,† Tianming Liu, PhD,‡ Martin Bues, PhD,* Mirek Fatyga, PhD,* and Wei Liu, PhD*

**Department of Radiation Oncology and †Division of Biostatics, Mayo Clinic Arizona, Phoenix, Arizona; and ‡Department of Computer Science, the University of Georgia, Athens, Georgia*

Received Aug 10, 2020, and in revised form Jan 25, 2021. Accepted for publication Feb 11, 2021.

Purpose: We proposed a novel tool—a dose linear energy transfer (LET)-volume histogram (DLVH)—and performed an exploratory study to investigate rectal bleeding in prostate cancer treated with intensity modulated proton therapy.

Methods and Materials: The DLVH was constructed with dose and LET as 2 axes, and the normalized volume of the structure was contoured in the dose-LET plane as isovolume lines. We defined the DLVH index, DLv%(d,l) (ie, v% of the structure) to have a dose of $\geq d$ Gy and an LET of $\geq l$ keV/μm, similar to the dose-volume histogram index Dv%. Nine patients with prostate cancer with rectal bleeding (Common Terminology Criteria for Adverse Events grade $\geq$2) were included as the adverse event group, and 48 patients with no complications were considered the control group. A P value map was constructed by comparison of the DLVH indices of all patients between the 2 groups using the Mann-Whitney U test. Dose-LET volume constraints (DLVCs) were derived based on the P value map with a manual selection procedure facilitated by Spearman's correlation tests. The obtained DLVCs were further cross-validated using a multivariate support vector machine (SVM)-based normal tissue complication probability (NTCP) model with an independent testing data set composed of 8 adverse event and 13 control patients.

Corresponding author: Wei Liu, PhD; E-mail: liu.wei@mayo.edu

This research was supported by an Arizona Biomedical Research Commission Investigator Award, the Lawrence W. and Marilyn W. Matteson Fund for Cancer Research, and the Kemper Marley Foundation.

Disclosures: W.L. reports grants from NIH/NCI outside the submitted work; in addition, W.L. has a pending U.S. patent: "An Accurate and Efficient Hybrid Method Based on Ray Casting to Calculate Physical Dose and Linear Energy Transfer (LET) Distribution for Intensity modulated Proton Therapy," which is licensed to .decimal LLC. S.E.S. reports personal fees from being an UpToDate editor and author outside the submitted work. T.L. reports grants from NSF and NIH (NSF CRCNS IIS-2011369, NIH R01 AG-042599, NIH R01 DA-033393, NSF CAREER Award IIS-1149260, NSF BME Core Program: CBET-1302089, NSF Cognitive Neuroscience Core Program: BCS-1439051, NSF Advances in Biological Informatics [ABI] Program: DBI-1564736, NIH Career Award: K01 EB-006878, NIH R01 HL-08792), outside the submitted work.

Data sharing statement: Research data are stored in an institutional repository. Some of the data can be shared upon request to the corresponding author.

Supplementary material for this article can be found at https://doi.org/10.1016/j.ijrobp.2021.02.024.

Int J Radiation Oncol Biol Phys, Vol. 110, No. 4, pp. 1189–1199, 2021
0360-3016/$ - see front matter
https://doi.org/10.1016/j.ijrobp.2021.02.024

Results: We extracted 2 DLVC constraints. One DLVC was obtained, $V\left(\text{dose/LET boundary}: 2.5\frac{\text{keV}}{\mu\text{m}} \text{ at } 75 \text{ Gy to } 3.2\frac{\text{keV}}{\mu\text{m}} \text{ at } 8.65 \text{ Gy}\right) < 1.27\%$ (DLVC1), revealing a high LET volume effect. The second DLVC, $V\left(72.2 \text{ Gy}, 0\frac{\text{keV}}{\mu\text{m}}\right) < 2.23\%$ (DVLC2), revealed a high dose volume effect. The SVM-based NTCP model with 2 DLVCs provided slightly superior performance than using dose only, with an area under the curve of 0.798 versus 0.779 for the testing data set.

Conclusions: Our results demonstrated the importance of rectal "hot spots" in both high LET (DLVC1) and high dose (DLVC2) in inducing rectal bleeding. The SVM-based NTCP model confirmed the derived DLVCs as good predictors for rectal bleeding when intensity modulated proton therapy is used to treat prostate cancer.

Introduction

Intensity modulated proton therapy (IMPT) provides highly conformal tumor target coverage while sparing adjacent organs at risk (OARs), thus reducing possible adverse events (AEs).[1-7] The relative biological effectiveness (RBE) dose of proton therapy is not only related to its physical dose but is also highly dependent on the average energy loss in a short distance traveled by protons, known as linear energy transfer (LET).[8] Compared with LET of traditional photon radiation therapy, the LET of protons increases dramatically with the deceleration of the protons and thus is typically high at the end of the proton ranges. Various LET-guided plan optimization methods have been proposed to improve potential clinical outcomes.[9-19]

Although variation in RBE induced by LET has been well recognized in the proton therapy community,[20] the precise relation of RBE and LET is still unclear.[21] In clinical practice, a constant RBE of 1.1 is widely adopted as a coarse approximation to describe the effect of protons compared with photons.[20] To study the possibility that a variable RBE is involved owing to LET, numerous in vitro[9,20,22-24] and in vivo[25-28] experiments have been carried out, and a number of phenomenological RBE models[12,21,29-34] and mechanism-related models[35-40] have been proposed. Most of these phenomenological models are developed based on the linear-quadratic equation. The LET effect is assumed as a function of cell radiation sensitivity change (α and β values) due to protons, and their coefficients relative to photons are obtained by fitting the in vitro clonogenic cell survival data. However, systematic comparisons revealed considerable variation among in vitro experimental results and consequently in the RBE estimations using different models.[41] In fact, clinical outcome data showed ambiguous results regarding the effect of LET.[25-27,42] The RBE of proton therapy is dependent on many factors (eg, LET, clinical endpoints, tissue type, fractionation scheme, patient-specific radiosensitivity, physical dose[11,20] the uncertainties in experimental measurements[10,30,32,33,43,44]). Although there are many uncertainties, the RBE of protons monotonically increases with LET when all other parameters are held the same.[30,45] Thus, LET can be considered as a surrogate of RBE.

Dose-volume histograms (DVHs) summarize 3-dimensional (3D) dose distributions in a graphical 2-dimensional (2D) format,[46] which simplifies 3D dose distributions by sacrificing spatial information. Dose-volume constraints (DVCs) based on population studies of patient outcomes[47,48] were routinely used as objectives to be met when designing treatment plans. However, DVC-based treatment planning exclusively optimizes dose distributions only. A new tool that integrates both physical dose and LET is needed to evaluate the biologic effects of proton radiation therapy.

In this exploratory study, we developed dose-LET volume histograms (DLVHs), which are conceptually similar to DVHs. We added LET as a new independent dimension in this novel tool. Because DLVH includes both dose and LET as independent variables, for proof of concept we now have a tool to study the correlations of clinical outcomes to not only the traditional dose parameter but also the LET parameter.

Methods and Materials

DLVH

We developed a new tool, the DLVH, to present both dose and LET distributions within a structure. DLVHs were constructed with physical dose (in Gy) and LET (in keV/μm) as 2 axes, and the third dimension is the normalized volume. Similar to the definition of DVH, the normalized volume is calculated as

$$V_{D,LET}(d,l) = V(D \geq d,\ LET \geq l) \quad (1)$$

where the right-hand side represents the cumulative normalized volume that has a value of dose, D, of at least d (Gy) and a value of LET, L, of at least l (keV/μm). The DLVH concept is similar to DVH, but it is a 3D cumulative volume histogram, rather than 2D as in the DVH. It contains an additional independent dimension, LET. DLVH thus differentiates itself from the DVH and LET-volume histogram (LETVH) and their simple multiplication.

The normalized volume of the structure is represented by isovolume curves contoured in the dose-LET plane. An example of DLVHs with 1%, 5%, 10%, and 20% isovolume lines is shown in Figure 1. Similar to DVH indices such as Dv%, these isovolume lines, notated as DLv%, represent the percentage volume of a structure that has a dose (D) of at least d Gy and an LET (L) of at least l keV/μm. For example, the orange cross on the $DL_{1\%}$ line in Figure 1 indicates that 1% of the rectum has a dose of at least 75

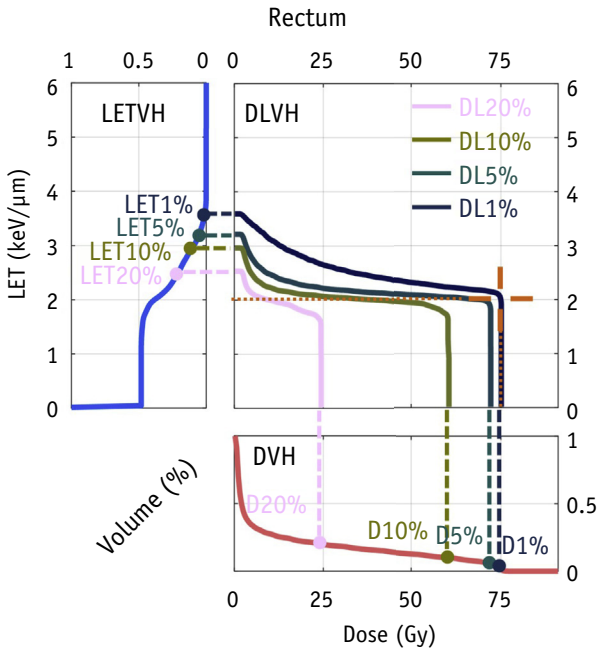

Fig. 1. Dose-linear-energy-transfer (LET) volume histogram (DLVH). Example of DLVH in rectum. DLv% lines (solid lines with different colors) represent the percentage volume of a structure that has a dose of at least d Gy and an LET of at least l keV/μm. The orange cross on the DL1% line indicates that 1% of the rectum has a dose of at least 75 Gy and an LET of at least 2 keV/μm. In DLVH, the conventional dose-volume histogram (DVH) (bottom panel) is presented as the line of $l = 0$, whereas the LET-volume histogram (LETVH; left panel) is presented as the line of $d = 0$. The intersections of DL lines with the dose and LET axes are Dv% in DVH and LETv% in LETVH, respectively. (A color version of this figure is available at https://doi.org/10.1016/j.ijrobp.2021.02.024.)

Gy and an LET of at least 2 keV/μm. This plot allows a straightforward and quantitative illustration of how the dose and LET are distributed and interplay within the selected structure. The conventional DVH can be extracted as a special case of DLVH, that is, as a line of $l = 0$ (the x-axis) (Fig. 1, bottom). Similarly, the LETVH[19] is a special case of DLVH with $d = 0$ (Fig. 1, left). Hence, the intersections of DL lines with the dose and LET axes are Dv% in DVH and LETv% in LETVH, respectively.

In our current investigation, we used 64 bins for both the dose (1.42 Gy per bin) and LET (0.156 keV/μm per bin) dimensions in the DLVH calculation. To get the optimal number of bins with a good balance of computing burden, statistical noise, and fine feature presentation, various experiments were performed by varying the number of bins in the x- and y-axis of the DLVH plot. We found that with 64 bins in the x- and y-axis of the DLVH plot, DLVH can still present distinguishable fine features with an acceptable statistical noise level at each bin and with a reasonable computation burden. Note that we present the data related to physical dose in units of Gy, rather than Gy[RBE], to avoid inclusion of the assumed RBE value. Patient prescription doses are still presented assuming a fixed RBE of 1.1 to follow clinical practice.

Patient cohort and IMPT treatment planning

This study was approved by our institution research board with institution research board number 13-005709. In this study, we included patients with prostate cancer treated in the definitive setting with conventional dose fractionation (75.6 Gy[RBE = 1.1] to 79.2 Gy[RBE = 1.1] in 42-44 fractions). A total of 117 patients were found. Out of these patients, we only included patients treated with a plan composed of alternating left and right fields (see the treatment planning details in the following sections). Patients were excluded if they (1) received a boost dose within the prostate, (2) were postprostatectomy, and (3) had lymph node and/or adjacent organ involvement with tumor. Concomitant androgen deprivation therapy was allowed for patients as determined by the treating physician. To make the plans as consistent as possible, we only included plans generated using Varian Eclipse v13.7 (Varian Medical Systems, Palo Alto, CA). Nine patients with prostate cancer with chronic rectal bleeding (Common Terminology Criteria for Adverse Events grade $\geq$2) were identified as the AE group and confirmed through the electronic medical record by an independent radiation oncologist. The AE group patients were treated between September 2016 and September 2017. For the control group, we nonselectively included all 48 patients who were treated during the same period and did not develop rectal bleeding (Table 1; more details in Table E1).

The plan was optimized using single-field optimization with 1 field from the left and the other from the right. Each field was optimized to the full prescription dose and delivered separately on alternating days.[49] At the discretion of the treating physician, hydrogel spacers were placed before treatment for some patients to increase the physical separation between the prostate and anterior rectal wall.[50,51] No statistically significant difference between the 2 groups was observed in age, spacer application, or concomitant androgen deprivation therapy (Table 1). All IMPT plans were reviewed and approved by experienced physicists and physicians to ensure that the institutional DVCs were met (Table E2).

Dose and LET calculation

The dose and LET distributions of the corresponding IMPT plan were calculated by the in-house developed fast Monte Carlo dose/LET calculation engine with the minimum energy cutoff of 50 keV.[52] This Monte Carlo dose engine has been carefully commissioned and benchmarked, which is used clinically as our second monitor unit check system. The total dose was computed by voxel-wise summation of dose distributions from 2 fields. The final LET was obtained

Table 1 Summary and statistical test results of patients, treatment, and tumor characteristics for the entire cohort and the AE group

	Median (range)				
	Total	AE group	Ctr group	Statistical test	*P* value
Age, y	72 (64-84)	76 (64-81)	72 (65-84)	Mann-Whitney U test	.119
Gleason score	7 (6-9)	7 (7-9)	7 (6-9)	Mann-Whitney U test	.919
	Positive counts/all counts			Statistical test	*P* value
	Total	AE group	Ctr group		
SpaceOAR	32/57	3/9	29/48	χ^2 test	.132
Chemotherapy	0/57	0/9	0/48	χ^2 test	*
Hormonal therapy	36/57	7/9	29/48	χ^2 test	.322

Abbreviations: AE = adverse events; Ctr = control; OAR = organs at risk.
* No patient in positive group.

by voxel-wise summation of LET distributions from 2 fields weighted by the corresponding dose (Fig. 2a).[53]

Statistical analysis and DLVC extraction

We used the cumulative normalized volume, $V_{D,LET}(d,l)$, as the DLVH indices for the rectal bleeding study. Dose and LET were binned in 64 bins for each dimension, and a total of 4096 $V_{D,LET}(d,l)$ were compared between the AE group and control group using the Mann-Whitney U test. The resulting *P* values $p(d,l)$ from all indices were displayed on the dose-LET plane to form a *P* value map (Fig. 3a).

We extracted the DLVCs by analyzing the *P* value map features. Initially, the dose and LET values of DLVCs were extracted by finding the local minimum in the *P* value map (colored dots in Fig. 3a). These DLVH indices indicated the most statistically significant metrics that can distinguish the 2 groups. DLVH indices with low *P* values were considered as potential candidates for DLVCs (Table E3). Because the candidate DLVH indices could be redundant and intercorrelated, it is important to find the metrics with minimum redundancy and maximum independence as DLVCs.

In this exploratory study, a manual selection procedure was carried out as in the conventional DVH-based patient outcome study. Spearman's correlation tests were performed to examine the correlation among all 4096 DLVH indices and the selected DLVH indices. Spearman's correlation coefficient maps for the candidate DLVH indices were constructed by presenting the calculated correlation coefficients in 2 dimensions with the x-axis as physical dose and the y-axis as LET, just as in the *P* value map (Fig. 3c).

We fine-tuned the DLVCs by selecting candidate DLVH indices and combining relevant candidate indices based on the overall performance as well as their clinical implications (for details of fine tuning DLVCs, see Materials E1). Volume threshold at the optimal operating point of the receiver operating characteristic (ROC) curve was used as the volume constraint for each DLVC. Area under the curve (AUC) of the ROC curve was calculated to evaluate the performance of each derived DLVC. A similar DLVC extraction process using the absolute volume was also performed, in which similar DLVCs were derived. Statistical results were generated using Matlab 2019a (MathWorks, Inc, Natick, MA).

DLVC-based normal tissue complication probability modeling

To validate the derived DLVCs, we established a multivariate support vector machine (SVM)-based normal tissue complication probability (NTCP) model based on the derived DLVCs via sequential minimal optimization to minimize an objective function as follows

$$\min_{\boldsymbol{w},b,\xi}\left(\frac{1}{2}\boldsymbol{w}^2+C\sum_i\xi_i\right), \tag{2}$$

$$s.t.y_i\left(\boldsymbol{w}^T\cdot\boldsymbol{V}^i_{\boldsymbol{d},\boldsymbol{l}}+b\right)\geq 1-\xi_i$$

$$\xi_i\geq 0$$

where $\boldsymbol{V}^i_{\boldsymbol{d},\boldsymbol{l}}=(V_{d_1,l_1}{}^i,\ V_{d_2,l_2}{}^i)$ is a vector of the DLVCs from patient i, $\boldsymbol{w}$ and b are the weights and intercept for the linear combination of features V_{d_1,l_1}, V_{d_2,l_2}, ξ_i is the slack variable to relax the margin for misclassifications with penalty parameter C, and y_i is the observed binary class variable of patient i, which is set to be 1 for the AE group and -1 for the control group. In this study, the penalty weight of misclassifying patients in the AE group was set as 4 times larger than the one in the control group, considering the imbalance of the patient sample numbers (for details, please see Materials E2). The SVM model has been calibrated using Platt scaling. The estimated NTCP was the posterior probability of the SVM model by fitting a sigmoid function using the leave-one-out cross-validation method.

The AUCs with 95% confidence intervals of the ROC curves for the leave-one-out cross validation tests were calculated from the SVM-based NTCP model to assess the performance. To test the SVM model and compare it to the performance of the conventional generalized equivalent uniform dose (gEUD)-based model (Materials E2), we have

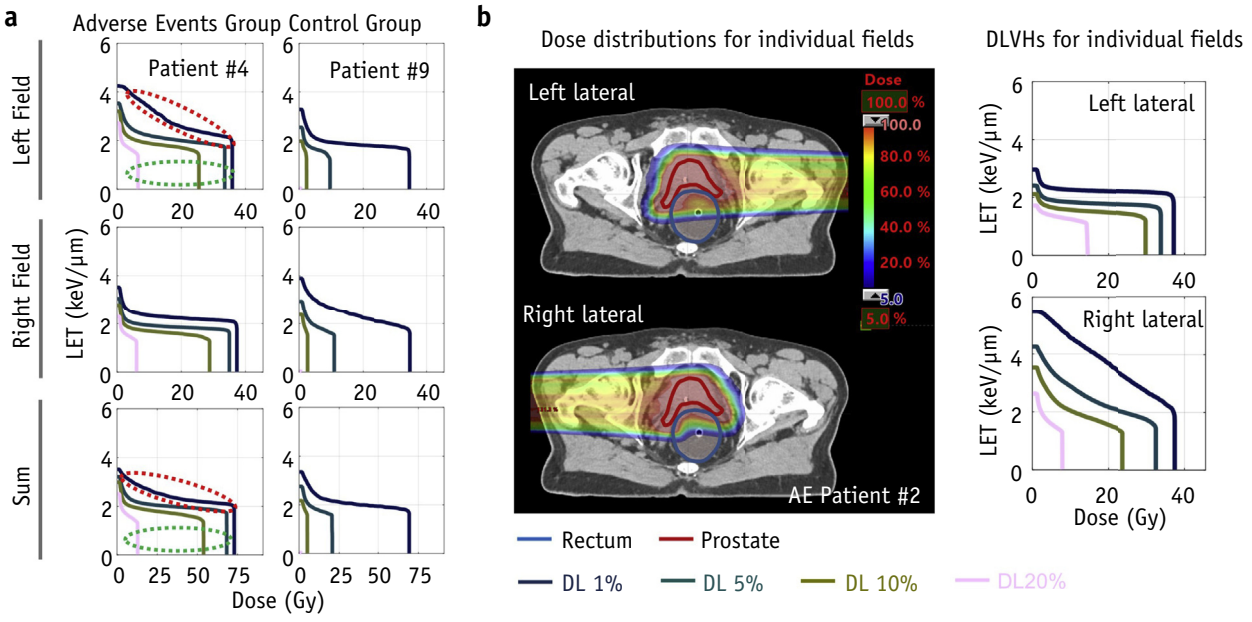

Fig. 2. Dose-linear-energy-transfer (LET) volume histogram (DLVH) from individual fields and sum plan between the 2 groups. (a) Comparison of typical DLVHs of the adverse event (AE) group (left panel) and the control group (right panel) from individual fields and sum plan with the dose-averaged LET. Compared with the AE group, DL5%, DL10%, and DL20% lines in the control group appear in significantly lower dose regions (indicated as green oval). DL1% line with higher LET is also seen in the AE group (indicated as red oval). (b) Dose distribution from left field (left top panel) and right field (left bottom panel) from a representative patient experiencing rectal bleeding. The prostate is contoured in the red line, and the rectum is contoured in the blue line. DLVHs (DL1%, DL5%, DL10%, and DL20%) of left field (right top panel) and right field (right bottom panel) were plotted. Asymmetry of DLVHs from both fields is shown. (A color version of this figure is available at https://doi.org/10.1016/j.ijrobp.2021.02.024.)

included an additional, independent testing patient group composed of 8 patients with rectal bleeding and 13 control patients who were treated during September 2017 to December 2017 to validate the effectiveness of the model. These 8 patients with rectal bleeding were treated with different fractionation schemes from the patients included in the model training. We thus rescaled to the physical doses of these patients using the equivalent dose at fractionation of 1.8 Gy[RBE = 1.1] assuming an α/β ratio of 3.0 for rectum. The control patients were nonselectively chosen for all 79.2 Gy[RBE = 1.1]/44 fractions with 2 alternating lateral fields. Testing results were evaluated with AUCs and compared. Modeling, including training, validation, and testing, was performed using Matlab 2019a as well.

Results

DLVHs of individual fields and sum plan between the 2 groups

We first examined the DLVHs of individual alternating fields (Fig. 2a). Compared with DLVHs from the control group (Fig. 2a, right column), DLVHs from the AE group (Fig. 2a, left panel) showed several dosimetric features: (1) DL5%, DL10%, and DL20% lines appeared higher in the low-LET regions (high dose-volume effect, indicated as the green oval in Fig. 2a); (2) higher LET volume was seen in the DLVHs of 1 of the alternating fields in the AE group (indicated as the red oval in Fig. 2a); (3) asymmetry of DLVHs between the left (Fig. 2a, top) and right field (Fig. 2a, middle) was observed in the AE group (indicated as the difference of DLVHs between the 2 alternating fields in Fig. 2a). The DLVHs with the dose-averaged LET (sum plan) (Fig. 2a, bottom) had features similar to the DLVHs of the corresponding individual fields, but the LET was generally reduced by the dose-weighted averaging from both fields.

We show the 3D dose distributions of a patient with rectal bleeding in Figure 2b (left). The high LET volume effect and the asymmetry in DLVHs between the 2 alternating fields (Fig. 2b, right) may result from the asymmetrical prostate anatomy of this patient (Fig. 2b, left), possibly due to the off-center placement of the hydrogel spacer. The spots from 1 field may stop at the distal end of the target, which may lead to high LET in the rectum passing by. However, the underlying mechanism was unclear, and this observation warrants further investigation.

DLVH indices

To quantitatively investigate the difference in DLVHs between these 2 groups, we statistically tested all 4096 DLVH

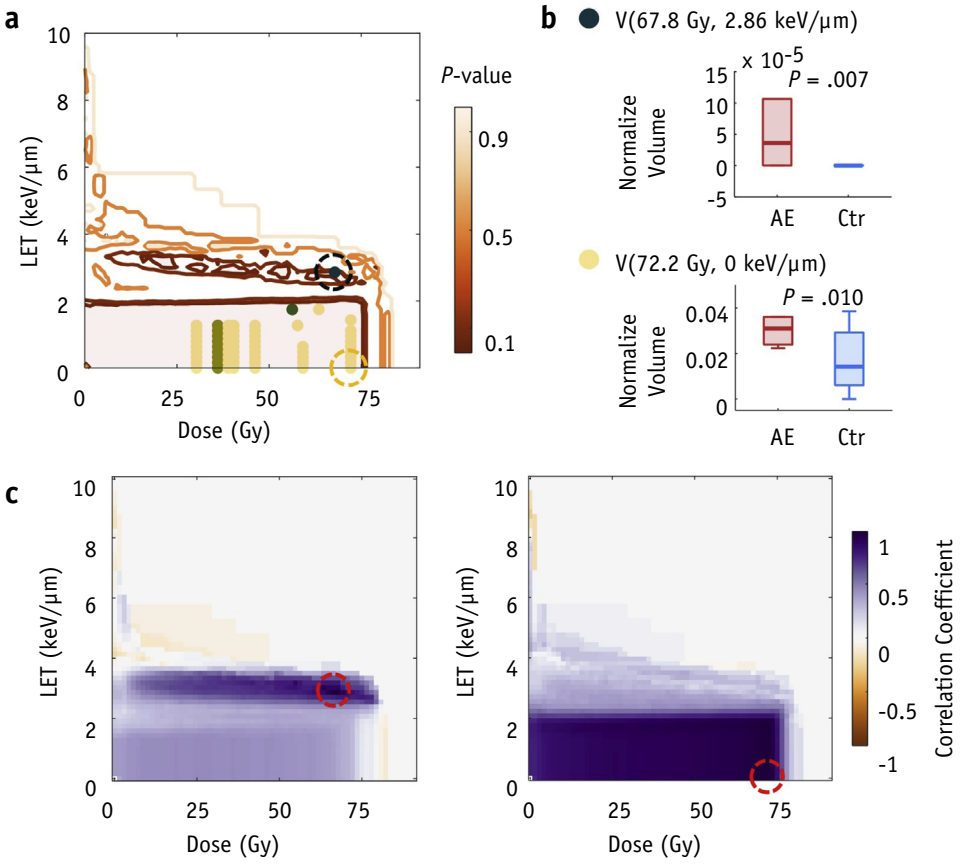

Fig. 3. Dose-linear-energy-transfer (LET) volume constraints (DLVC) extraction and fine tuning. (a) P value map of dose-LET volume histogram (DLVH) indices in the dose-LET plane. Contoured P value map of DLVH indices of $P = .05$, 0.1, 0.5, and 0.9. Shaded area in light red indicates areas with $P < .05$ (from the Mann-Whitney U test). Local minima of P values are indicated as scatter points with different colors. (b) Box plot of 2 candidate DLVH indices (circled in 3a). Both showed statistical significance. (c) Spearman's coefficient map of the 2 candidate DLVH indices (circled in red). High correlation coefficients were observed for high-LET and high-dose regions, respectively, but relatively small correlations were obtained between these 2 regions. (A color version of this figure is available at https://doi.org/10.1016/j.ijrobp.2021.02.024.)

indices, $V_{D,LET}(d,l)$, of the sum plans with the dose-averaged LET using Mann-Whitney U test between 2 groups. We generated a P value map by reconstructing the resulting P values, $p(d,l)$, for each dose/LET bin (d,l) after the statistical tests (Fig. 3a). Results revealed 2 main areas with statistical significance ($P < .05$). One was located at low LET over a large dose span (big red shadow regions in Fig. 3a). The other one was at high LET with several $P < .05$ islands (small red shadow regions). The dose LET volume distributions, $V_{D,LET}(d,l)$, in these regions were significantly different between the 2 groups. We highlighted multiple DLVH indices of $P < .01$ as colored dots in Figure 3a by finding the local minimums in the P value map (different colors indicate different P values: darker colors indicate smaller P values, with raw data in Table E3). Figure 3b shows box plots of 2 DLVH indices for both high-LET and low-LET regions: $V(67.8\ Gy,\ 2.86\ keV/\mu m)$ (Fig. 3b, top) and $V(72.2\ Gy,\ 0\ keV/\mu m)$ (Fig. 3b, bottom), circled in Figure 3a. Their volume distributions were significantly higher in the patients with AE at both indices ($V\left[67.8\ Gy,\ 2.86\frac{keV}{\mu m}\right]$: $P = .007$; $V\left[72.2\ Gy,\ 0\frac{keV}{\mu m}\right]$, $P = .010$). These observations were consistent with the raw DLVHs displayed in Figure 2. Therefore, both high dose volume and high LET volume were statistically significant features between the 2 groups.

Note that DLVH indices were highly redundant. This can be seen as the same P values are aligned over multiple LET bins at the same dose (Fig. 3a). To understand the relationship of these DLVH indices, we studied correlations between DLVH indices using Spearman's correlation for all patients and generated 2 correlation coefficient maps for all DLVH indices in reference to the 2 DLVH indices, $V(67.8\ Gy,\ 2.86\ keV/\mu m)$ (Fig. 3c, left) and $V(72.2\ Gy,\ 0\ keV/\mu m)$ (Fig. 3c, right), circled in Figure 3a. DLVH indices at high LET (Fig. 3c, left) and low LET (Fig. 3c, right) achieved a high correlation coefficient (>0.6) to the 2 reference DLVH indices, respectively, whereas the correlation between 2 regions was low (a coefficient of 0.293 between 2 reference DLVH indices was observed). These results strongly suggest that the low-LET and high-LET DLVH

indices were relatively independent, and indices within each region were highly correlated. Thus, metrics at these 2 regions represented 2 distinct dosimetric features that could be involved in rectal bleeding. DLVH indices at low LET mainly reflected the high-dose volume in the rectum, whereas DLVH metrics at high LET represented the high-LET volume in the rectum.

DLVC extraction from DLVH indices

It is important to minimize the redundancy and maximize the independence of DLVH metrics to derive DLVCs. Considering the robustness of the derived DLVC and its clinical implications, we combined metrics in high-LET regions and obtained DLVC1 (see Materials E3). DLVC1 was defined by a curve in the dose-LET plane determined according to the iso-*P* value line of 0.1 (Fig. 1). The lower LET boundary was close to 2.5 keV/μm at 75 Gy and gradually increased to 3.2 keV/μm at 8.65 Gy. The lower dose boundary was close to 8.65 Gy. By analyzing the ROC performance, we obtained an optimal volume threshold for DLVC1, $V\left(\frac{\text{dose}}{\text{LET}}\text{boundary: } 2.5\frac{\text{keV}}{\mu\text{m}}\text{at 75 Gy to } 3.2\frac{\text{keV}}{\mu\text{m}}\text{at 8.65 Gy}\right) < 1.27\%$ or 1.71 cc. DLVC1 indicated a quantitative high LET volume effect to rectal bleeding. It suggested that with sufficiently high LET and the corresponding dose determined by the aforementioned dose-LET curve, the volume enclosed by such a dose-LET curve should be less than 1.27% or 1.71 cm^3 to prevent rectal bleeding. This is very similar to the current routine clinical practice in the evaluation of biological effects of IMPT plans to treat prostate cancer at our institution (ie, to avoid the overlap of high LET and high dose in OARs as much as possible). However, compared with our current clinical practice, the derived DLVC1 was quantitative and purely based on patient outcomes.

Low-LET DLVC revealed a high dose volume effect related to rectal bleeding, with no or little effect from LET. According to quantitative analysis of normal tissue effects in the clinic (QUANTEC)[47] and our institutional practice, multiple DVCs were employed during treatment planning (eg, V50 Gy[RBE = 1.1], V60 Gy[RBE = 1.1]). We found similar multiple metrics from DLVHs as observed in DL5%, DL10%, and DL20% lines in Figure 2a. Considering the robustness of the derived DLVC, we used $V(72.2\,Gy,\ 0\,keV/\mu m)$ as DLVC2. DLVC2 was only a dose-volume constraint, reflecting the high dose-volume effect related to rectal bleeding. We derived the volume constraint according to its ROC performance: $V(72.2\,Gy,\ 0\,keV/\mu m) < 2.23\%$ or $2.68\,cc$. The derived result was very close to the reported values[47] and the values used at our institutional dose volume constraints (D_{2cc} <79.5 Gy[RBE = 1.1]) for prostate cancer. The derived DLVC values from all patients are listed in Table E4.

DLVC validation using NTCP models

To validate the performance of both DLVCs and test the feasibility for multivariate NTCP models, we built a multivariate NTCP model with 2 DLVCs using SVM. The SVM-based NTCP model performance in training is displayed in Figure 4a and Figure E2. We further validated the model using the leave-one-out cross-validation method. The ROC curves of the validation results are shown in Figure 4b (Table 2 for results). The corresponding NTCP values and true classification of all 57 patients based on the SVM model in validation are shown in Figure 4c. Sensitivity of 0.67 and specificity of 0.69 were achieved at the NTCP cutoff value of 0.5 in validation (Fig. 4c). Decent performances were achieved for the SVM model for training (AUC_{SVM} = 0.785) and validation (AUC_{SVM} = 0.720).

We further evaluated the SVM model with the conventional gEUD-based univariate model[54] (Fig. E3). SVM outperformed gEUD in both the training (AUC_{SVM} = 0.785 vs AUC_{gEUD} = 0.762) and the leave-one-out cross validation (AUC_{SVM} = 0.720 vs AUC_{gEUD} = 0.704). The new model showed a slightly better outcome prediction and provided new perspective to the patient outcome study in proton therapy.

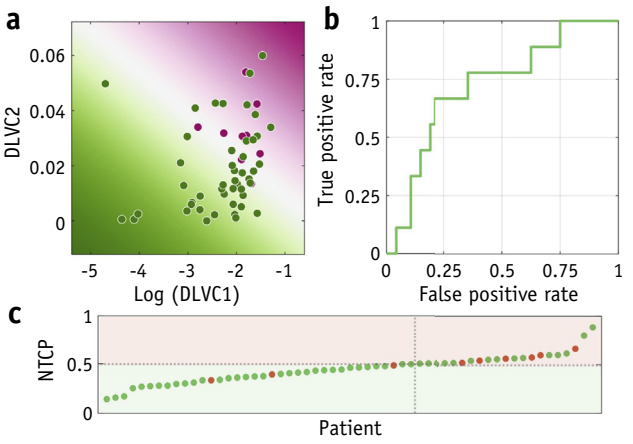

Fig. 4. Performance of support-vector-machine (SVM)-based normal tissue complication probability (NTCP) model. (a) Visualization of the trained NTCP model. Colored dots indicate the true patient outcome (pink dots indicate patients with rectal bleeding; green dots indicate control patients). The predicted NTCP score from the SVM NTCP model is colored in the plane of dose-linear-energy-transfer (LET) volume constraints (DLVCs). Dark pink indicates high NTCP and dark green indicates low NTCP, with white for NTCP = 0.5. (b) Receiver operating characteristic (ROC) curve of the leave-one-out cross validation from the SVM-based NTCP models. (c) NTCP prediction for all patients for the leave-one-out cross validation. Color of dots indicates the true patient outcome (red, rectal bleeding; green, no complications). The background indicates the prediction of the NTCP score below or above 0.5. (A color version of this figure is available at https://doi.org/10.1016/j.ijrobp.2021.02.024.)

Table 2 Performance of the NTCP models

	Training	Validation (Loocv)	Testing
Model*	AUC (95% CI)	AUC (95% CI)	AUC (95% CI)
SVM	0.785 (0.633-0.887)	0.720 (0.501-0.866)	0.798 (0.537-0.942)
gEUD	0.762 (0.614-0.875)	0.704 (0.480-0.822)	0.779 (0.441-0.950)

Abbreviations: AUC = area under the curve; CI = confidence interval; gEUD = generalized equivalent uniform dose; Loocv = leave-one-out cross validation; NTCP = normal tissue complication probability; SVM = support vector machine.
* gEUD model is based on logistic regression.

To further test the effectiveness of the SVM-based NTCP model, we included a patient cohort with 8 AE patients and 13 control patients as a testing data set. These patients were blind to the modeling process. Similar to the training and validation results, the SVM-based NTCP model achieved slightly better performance than the conventional gEUD-based NTCP model in testing (AUC_{SVM} vs AUC_{gEUD}: 0.798 vs 0.779, Table E5 for testing results of each patient and Fig. E3 for the ROC curve of the testing data), which indicated a consistently better performance from the new model.

Discussion

We developed a novel plan evaluation tool, DLVH, a 3D cumulative volume histogram including both dose and LET as independent variables, for analyzing AEs in patients with prostate cancer treated by IMPT (Fig. 1). Not only does this new tool present both dose and LET distributions individually as shown by DVH and LETVH, respectively, but it also provides information about their interplay, as shown by the joint dose-LET distributions within a structure in 1 illustration. Therefore, it provides more comprehensive information than the DVH alone.

In this exploratory study, we investigated the effect of LET without assuming any RBE model. To demonstrate the value of DLVH and investigate the possible effect of LET on the patients' AEs for proof of concept, we examined rectal bleeding in patients with prostate cancer treated by IMPT using DLVHs (Fig. 2). Patients who developed rectal bleeding were more likely to have high dose volume, high LET volume, and asymmetrical DLVHs between the left and right fields (Fig. 2a,b). These observations may have in part resulted from the asymmetrical prostate anatomy of these patients (Fig. 2b), possibly due to the off-center placement of the hydrogel spacer. However, the effect from this asymmetrical prostate geometry to the plan quality is undetermined and needs further investigation.

By testing cumulative normalized volume, $V_{D,LET}(d,l)$, as DLVH indices for all dose and LET bins, we confirmed the observation of high dose volume and high LET volume on the constructed P value map. The P value map showed 2 main regions on the dose-LET plane with $P < .1$, indicating high dose volume and high LET volume effect, respectively. Two DLVCs were identified for their association with rectal bleeding: V(dose/LET boundary: 2.5 $keV/\mu m$ at 75 Gy to 3.2 keV <1.27% or 1.71 cm^3 (DLVC1) and V(72.2 Gy, 0 keV μm) < 2.23% or 2.68 cm^3 (DLVC2). Spearman correlation tests revealed weak correlation between high-LET and low-LET DLVH indices (Fig. 3c), suggesting that these 2 DLVCs are relatively independent dosimetric features correlated to rectal bleeding.

The extracted DLVC1 is a curve on the dose-LET plane, suggesting an interplay effect between dose and LET. It is the first quantitative LET-related volume constraint that is purely based on patient outcomes. In our routine clinical practice to evaluate the biological effect of IMPT plans to treat prostate cancer, a volume enclosed by the iso-LET contour (ie, 6 keV/μm) is generated from the 3D LET distribution. One volume is generated by overlapping such a volume with a volume enclosed by 50% of the prescription iso-dose lines from the 3D dose distribution. This overlapping volume is checked carefully to make sure no overlapping exists in the nearby OARs.[55] The LET threshold (ie, 6 keV/μm) and the dose threshold (ie, 50% of the prescription dose) are arbitrary and entirely based on the rough estimates from physicists. In this work, we derived these thresholds quantitatively according to patient outcomes from the patients with documented rectal bleeding treated by IMPT.

The derived DLVC2 is more appropriate for comparison to the historical rectum DVCs. It indicates that a small volume of rectum receiving high dose is important in predicting rectal bleeding. This finding is consistent with various studies, such as QUANTEC,[47] and independent large-scale studies of patients with prostate cancer treated by proton therapy (V75 Gy[RBE = 1.1])[56] and photon therapy (V 72Gy).[57] The obtained rectum volume constraint is also very close to the value used at our institution for photon therapy. Thus, the consistency with the literature further validated the effectiveness of the proposed DLVH method for IMPT plan evaluation.

In this study, we fine-tuned DLVCs manually by combining or removing DLVH indices from a candidate DLVH index pool according to the P value map generated by the Mann-Whitney U test. A DLVH index (such as $V\left[67.8\ Gy,\ 2.86\frac{keV}{\mu m}\right]$) reveals hot spots at high dose and high LET in rectum, which was very predictive of rectal bleeding (dark blue dot in Fig. 3a). However, because very small volumes (1-2 voxels, 0.0032-0.0064 cm^3) may be

involved in this constraint, it suffers from large uncertainties from the dose and LET calculations and interpatient variations. Thus, it is not robust. Combining multiple DLVH indices (such as islands in Fig. 3a) helps improve the robustness of the prediction of the corresponding DLVCs with the cost of the prediction performance. Thus, as a proof-of-concept study, a manual selection was carried out in this initial work, which integrates clinical insight into the feature selection, avoids features due to artifacts from limited patient data, and improves the robustness of the selected features. This DLVC selection procedure can be further improved by various feature selection algorithms, such as principal component analysis, neighborhood component analysis, random-forest based methods, and so forth. This will be done in a future study.

We compared numerous DLVH indices to generate the *P*-map. To mitigate the type I error in multiple comparisons, we studied correlations among these indices to derive DLVCs. In addition, the permutation test method[58] can also be applied for this purpose. It randomly shuffles the labels between 2 groups and adjusts the *P* value using various correction methods. Because the *P* value map is employed to derive DLVCs for the NTCP modeling, global adjustment does not change the shape of the iso-*P* value lines and thus does not affect the procedure to derive DLVCs.

DLVCs can also be used as parameters to predict AEs for future patients. To demonstrate such capability and validate the efficacy of the derived DLVCs, we computed NTCPs based on DLVCs using the SVM model (Fig. 4). SVM outperforms the conventional gEUD-based model for training, validation, and testing, reflecting the merit of the SVM model prediction based on the derived DLVCs.

However, a limiting factor for this study is the size of the patient groups. In our institute, only ~7% of the patients with prostate cancer treated by IMPT experienced rectal bleeding after treatment. The increased model complexity requires more AE patients for training and validation. The performance of the current model indicated a marginal improvement of the conventional gEUD-based model based on the limited data set. With a larger amount of patient data becoming available, a more accurate NTCP model could be established, which will be done in a future study about rectal bleeding involving multiple institutions with efficient and secure data sharing enabled by some advanced algorithms such as blockchain.

The DLVH-based NTCP model for rectal bleeding in prostate cancer treated by IMPT as described in this manuscript has been integrated into Eclipse ver. 13.7 (Varian Medical Systems) as a plugin via Eclipse Scripting API and is ready for routine clinical use. Because of our highly automated clinical workflow and its user-friendly implementation, dosimetrists, after a couple of hours of training, can easily use the software and select the desired OAR to get the NTCP score by clicking the mouse several times. The result can be generated within a few minutes for typical prostate cancer plans owing to the highly parallelized software and the graphic processing unit-accelerated high-performance computing platform.

The reported model was based on our in-house developed fast Monte Carlo code, which is unfortunately not open source. However, we have also used an open-sourced Monte Carlo code, MCsquare,[59] to establish the DLVH-based NTCP model as described in this manuscript. MCsquare has been carefully benchmarked with our in-house developed fast Monte Carlo code. Excellent agreement between MCsquare and our in-house developed fast Monte Carlo code has been observed.[60] We have therefore built a similar model based on MCsquare. Good and consistent results were also achieved as with our in-house developed fast Monte Carlo code (results not reported here). We encourage other research groups to use MCsquare if they are interested in implementing similar tools at their proton clinics.

With a sensitivity of 0.67, a specificity of 0.69, and a prevalence of 7% (Fig. 4c), the chance that patients with prostate cancer treated by IMPT will develop rectal bleeding is 13.5% for those IMPT plans that have an NTCP score of $\geq$0.5. The chance will drop to 3.5% if the plan has an NTCP score of $\leq$0.5. The derived DLVCs can be further integrated into the treatment planning prospectively for better patient outcome via simultaneously constraining both LET and dose distributions. As a proof-of-principle study, we demonstrated the application of DLVH in rectal bleeding for patients with prostate cancer treated by IMPT.

It is unclear so far whether any RBE model can accurately predict the outcome of patients with cancer treated by proton therapy. What we may need instead is an empirical disease site− and organ-specific patient-outcome oriented model, which refrains from computing an equivalent photon dose required by the concept of RBE and, based on physical dose, LET, fractionation scheme, and so forth, directly calculates probabilities for tumor control and healthy tissue complication. We believe DLVH will be the first step in this direction and will be a powerful tool for patient outcome study in IMPT.

Conclusions

We developed a new tool, DLVH, for AE study in IMPT. For proof of concept, we applied this new tool to a rectal bleeding study in patients with prostate cancer treated by IMPT at our institution only. By comparing DLVHs of IMPT plans with rectal bleeding to plans without any complications, we derived 2 DLVCs that were relevant to rectal bleeding, 1 revealing high LET volume (DLVC1) and the other revealing high dose volume (DLVC2). We further validated the prediction power of the multivariate analysis with 2 DLVCs using the SVM-based NTCP model. The model achieved slightly better performance on training, validation, and testing compared with the model using gEUD alone. DLVH and DLVC can be powerful tools in patient outcome prediction in IMPT plan evaluation, and

they can be integrated into IMPT treatment planning to prospectively improve patient outcome.

References

1. Register SP, Zhang X, Mohan R, et al. Proton stereotactic body radiation therapy for clinically challenging cases of centrally and superiorly located stage i non-small-cell lung cancer. *Int J Radiat Oncol Biol Phys* 2011;80:1015-1022.
2. Stuschke M, Kaiser A, Pottgen C, et al. Potentials of robust intensity modulated scanning proton plans for locally advanced lung cancer in comparison to intensity modulated photon plans. *Radiother Oncol* 2012;104:45-51.
3. Zhang X, Li Y, Pan X, et al. Intensity-modulated proton therapy reduces the dose to normal tissue compared with intensity-modulated radiation therapy or passive scattering proton therapy and enables individualized radical radiotherapy for extensive stage IIIb non-small-cell lung cancer: A virtual clinical study. *Int J Radiat Oncol Biol Phys* 2010;77.
4. Frank SJ, Cox JD, Gillin M, et al. Multifield optimization intensity modulated proton therapy for head and neck tumors: A translation to practice. *Int J Radiat Oncol Biol Phys* 2014;89:846-853.
5. Liu C, Bhangoo RS, Sio TT, et al. Dosimetric comparison of distal esophageal carcinoma plans for patients treated with small-spot intensity-modulated proton versus volumetric-modulated arc therapies. *J Appl Clin Med Phys* 2019;20:15-27.
6. Liu C, Sio TT, Deng W, et al. Small-spot intensity-modulated proton therapy and volumetric-modulated arc therapies for patients with locally advanced non-small-cell lung cancer: A dosimetric comparative study. *J Appl Clin Med Phys* 2018;19:140-148.
7. Chang JY, Zhang X, Knopf A, et al. Consensus guidelines for implementing pencil-beam scanning proton therapy for thoracic malignancies on behalf of the PTCOG thoracic and lymphoma subcommittee. *Int J Radiat Oncol Biol Phys* 2017;99:41-50.
8. Belli M, Cera F, Cherubini R, et al. Rbe-let relationships for cell inactivation and mutation induced by low energy protons in v79 cells: Further results at the lnl facility. *Int J Radiat Biol* 1998;74:501-509.
9. Cao W, Khabazian A, Yepes PP, et al. Linear energy transfer incorporated intensity modulated proton therapy optimization. *Phys Med Biol* 2017;63:015013.
10. An Y, Shan J, Patel SH, et al. Robust intensity-modulated proton therapy to reduce high linear energy transfer in organs at risk. *Med Phys* 2017;44:6138-6147.
11. Unkelbach J, Botas P, Giantsoudi D, et al. Reoptimization of intensity modulated proton therapy plans based on linear energy transfer. *Int J Radiat Oncol Biol Phys* 2016;96:1097-1106.
12. Fager M, Toma-Dasu I, Kirk M, et al. Linear energy transfer painting with proton therapy: A means of reducing radiation doses with equivalent clinical effectiveness. *Int J Radiat Oncol Biol Phys* 2015;91:1057-1064.
13. Giantsoudi D, Grassberger C, Craft D, et al. Linear energy transfer-guided optimization in intensity modulated proton therapy: Feasibility study and clinical potential. *Int J Radiat Oncol Biol Phys* 2013;87:216-222.
14. Bassler N, Jakel O, Sondergaard CS, et al. Dose- and LET-painting with particle therapy. *Acta Oncologica* 2010;49:1170-1176.
15. Bassler N, Toftegaard J, Luhr A, et al. Let-painting increases tumour control probability in hypoxic tumours. *Acta Oncologica* 2014;53:25-32.
16. Inaniwa T, Kanematsu N, Noda K, et al. Treatment planning of intensity modulated composite particle therapy with dose and linear energy transfer optimization. *Phys Med Biol* 2017;62:5180-5197.
17. Bai X, Lim G, Grosshans D, et al. Robust optimization to reduce the impact of biological effect variation from physical uncertainties in intensity-modulated proton therapy. *Phys Med Biol* 2019;64:025004.
18. Traneus E, Oden J. Introducing proton track-end objectives in intensity modulated proton therapy optimization to reduce linear energy transfer and relative biological effectiveness in critical structures. *Int J Radiat Oncol Biol Phys* 2019;103:747-757.
19. Liu C, Patel SH, Shan J, et al. Robust optimization for intensity-modulated proton therapy to redistribute high linear energy transfer (let) from nearby critical organs to tumors in head and neck cancer. *Int J Radiat Oncol Biol Phys* 2020;107:181-193.
20. Paganetti H. Relative biological effectiveness (RBE) values for proton beam therapy. Variations as a function of biological endpoint, dose, and linear energy transfer. *Phys Med Biol* 2014;59:R419-R472.
21. Carabe A, Espana S, Grassberger C, et al. Clinical consequences of relative biological effectiveness variations in proton radiotherapy of the prostate, brain and liver. *Phys Med Biol* 2013;58:2103-2117.
22. Guan F, Bronk L, Titt U, et al. Spatial mapping of the biologic effectiveness of scanned particle beams: Towards biologically optimized particle therapy. *Sci Rep* 2015;5:9850.
23. Patel D, Bronk L, Guan F, et al. Optimization of Monte Carlo particle transport parameters and validation of a novel high throughput experimental setup to measure the biological effects of particle beams. *Med Phys* 2017;44:6061-6073.
24. Chaudhary P, Marshall TI, Perozziello FM, et al. Relative biological effectiveness variation along monoenergetic and modulated bragg peaks of a 62-mev therapeutic proton beam: A preclinical assessment. *Int J Radiat Oncol Biol Phys* 2014;90:27-35.
25. Gentile MS, Yeap BY, Paganetti H, et al. Brainstem injury in pediatric patients with posterior fossa tumors treated with proton beam therapy and associated dosimetric factors. *Int J Radiat Oncol Biol Phys* 2018;100:719-729.
26. Peeler CR, Mirkovic D, Titt U, et al. Clinical evidence of variable proton biological effectiveness in pediatric patients treated for ependymoma. *Radiother Oncol* 2016;121:395-401.
27. Underwood TSA, Grassberger C, Bass R, et al. Asymptomatic late-phase radiographic changes among chest-wall patients are associated with a proton rbe exceeding 1.1. *Int J Radiat Oncol Biol Phys* 2018;101:809-819.
28. Bolsi A, Placidi L, Pica A, et al. Pencil beam scanning proton therapy for the treatment of craniopharyngioma complicated with radiation-induced cerebral vasculopathies: A dosimetric and linear energy transfer (let) evaluation. *Radiother Oncol* 2020;149:197-204.
29. Beltran C, Tseung HWC, Augustine KE, et al. Clinical implementation of a proton dose verification system utilizing a GPU accelerated monte carlo engine. *Int J Part Ther* 2016;3:312-319.
30. Wilkens JJ, Oelfke U. A phenomenological model for the relative biological effectiveness in therapeutic proton beams. *Phys Med Biol* 2004;49:2811-2825.
31. Frese MC, Wilkens JJ, Huber PE, et al. Application of constant vs. variable relative biological effectiveness in treatment planning of intensity-modulated proton therapy. *Int J Radiat Oncol Biol Phys* 2011;79:80-88.
32. Wedenberg M, Lind BK, Hardemark B. A model for the relative biological effectiveness of protons: The tissue specific parameter alpha/beta of photons is a predictor for the sensitivity to let changes. *Acta Oncologica* 2013;52:580-588.
33. McNamara AL, Schuemann J, Paganetti H. A phenomenological relative biological effectiveness (RBE) model for proton therapy based on all published in vitro cell survival data. *Phys Med Biol* 2015;60:8399-8416.
34. Rørvik E, Thörnqvist S, Stokkevåg CH, et al. A phenomenological biological dose model for proton therapy based on linear energy transfer spectra. *Med Phys* 2017;44:2586-2594.
35. Hawkins RB. A microdosimetric-kinetic model for the effect of non-poisson distribution of lethal lesions on the variation of RBE with LET. *Radiat Res* 2003;160:61-69.
36. Schulz-Ertner D, Karger CP, Feuerhake A, et al. Effectiveness of carbon ion radiotherapy in the treatment of skull-base chordomas. *Int J Radiat Oncol Biol Phys* 2007;68:449-457.
37. Elsässer T, Scholz M. Cluster effects within the local effect model. *Radiat Res* 2007;167:319-329.

38. Elsässer T, Krämer M, Scholz M. Accuracy of the local effect model for the prediction of biologic effects of carbon ion beams in vitro and in vivo. *Int J Radiat Oncol Biol Phys* 2008;71:866-872.
39. Elsässer T, Weyrather WK, Friedrich T, et al. Quantification of the relative biological effectiveness for ion beam radiotherapy: Direct experimental comparison of proton and carbon ion beams and a novel approach for treatment planning. *Int J Radiat Oncol Biol Phys* 2010; 78:1177-1183.
40. Carlson DJ, Stewart RD, Semenenko VA, et al. Combined use of Monte Carlo DNA damage simulations and deterministic repair models to examine putative mechanisms of cell killing. *Radiat Res* 2008;169:447-459.
41. Rørvik E, Fjæra LF, Dahle TJ, et al. Exploration and application of phenomenological rbe models for proton therapy. *Phys Med Biol* 2018;63:185013.
42. Berrington de Gonzalez A, Vikram B, Buchsbaum JC, et al. A clarion call for large-scale collaborative studies of pediatric proton therapy. *Int J Radiat Oncol Biol Phys* 2017;98:980-981.
43. Carabe A, Moteabbed M, Depauw N, et al. Range uncertainty in proton therapy due to variable biological effectiveness. *Phys Med Biol* 2012;57:1159.
44. Grün R, Friedrich T, Krämer M, et al. Systematics of relative biological effectiveness measurements for proton radiation along the spread out bragg peak: Experimental validation of the local effect model. *Phys Med Biol* 2017;62:890.
45. Guan F, Peeler C, Bronk L, et al. Analysis of the track-and dose-averaged let and let spectra in proton therapy using the geant4 Monte Carlo code. *Med Phys* 2015;42:6234-6247.
46. Drzymala RE, Mohan R, Brewster L, et al. Dose-volume histograms. *Int J Radiat Oncol Biol Phys* 1991;21:71-78.
47. Bentzen SM, Constine LS, Deasy JO, et al. Quantitative analyses of normal tissue effects in the clinic (QUANTEC): An introduction to the scientific issues. *Int J Radiat Oncol Biol Phys* 2010;76:S3-S9.
48. Emami B, Lyman J, Brown A, et al. Tolerance of normal tissue to therapeutic irradiation. *Int J Radiat Oncol Biol Phys* 1991;21:109-122.
49. Kirk ML, Tang S, Zhai H, et al. Comparison of prostate proton treatment planning technique, interfraction robustness, and analysis of single-field treatment feasibility. *Pract Radiat Oncol* 2015;5: 99-105.
50. Hamstra DA, Mariados N, Sylvester J, et al. Continued benefit to rectal separation for prostate radiation therapy: Final results of a phase iii trial. *Int J Radiat Oncol Biol Phys* 2017;97:976-985.
51. Navaratnam A, Cumsky J, Abdul-Muhsin H, et al. Assessment of polyethylene glycol hydrogel spacer and its effect on rectal radiation dose in prostate cancer patients receiving proton beam radiation therapy. *Adv Radiat Oncol* 2020;5:92-100.
52. Tseung HWC, Ma J, Beltran C. A fast gpu-based monte carlo simulation of proton transport with detailed modeling of nonelastic interactions. *Med Phys* 2015;42:2967-2978.
53. Deng W, Ding X, Younkin JE, et al. Hybrid 3d analytical linear energy transfer calculation algorithm based on precalculated data from monte carlo simulations. *Med Phys* 2019;47:745-752.
54. Niemierko A. A generalized concept of equivalent uniform dose (eud). *Med Phys* 1999;26:1100.
55. Deng W, Yang Y, Liu C. A critical review of let-based intensity-modulated proton therapy (impt) plan evaluation and optimization for head and neck cancer management. *Int J Part Ther* 2020. In press.
56. Colaco RJ, Hoppe BS, Flampouri S, et al. Rectal toxicity after proton therapy for prostate cancer: An analysis of outcomes of prospective studies conducted at the university of florida proton therapy institute. *Int J Radiat Oncol Biol Phys* 2015;91:172-181.
57. Vargas C, Martinez A, Kestin LL, et al. Dose-volume analysis of predictors for chronic rectal toxicity after treatment of prostate cancer with adaptive image-guided radiotherapy. *Int J Radiat Oncol Biol Phys* 2005;62:1297-1308.
58. Chen C, Witte M, Heemsbergen W, et al. Multiple comparisons permutation test for image based data mining in radiotherapy. *Radiat Oncol* 2013;8:293.
59. Souris K, Lee JA, Sterpin E. Fast multipurpose monte carlo simulation for proton therapy using multi- and many-core CPU architectures. *Med Phys* 2016;43:1700-1712.
60. Deng W, Younkin JE, Souris K, et al. Technical note: Integrating an open source monte carlo code "mcsquare" for clinical use in intensity-modulated proton therapy. *Med Phys* 2020;47:2558-2574.